# State of Charge-Dependent Polynomial Equivalent Circuit Modeling for Electrochemical Impedance Spectroscopy of Lithium-Ion Batteries

Qian-Kun Wang, Yi-Jun He, Jia-Ni Shen, Xiao-Song Hu, *Senior Member, IEEE*, and Zi-Feng Ma

***Abstract*—Electrochemical impedance spectroscopy (EIS) is used not only to give a thorough understanding of reaction kinetics and transport mechanisms in lithium-ion batteries (LIBs), but also to provide a promising nondestructive tool for state of charge (SOC) estimation. Although various equivalent circuit models (ECMs) have been proposed to model impedance spectra, the impact of SOC on circuit parameters is often neglected in these models. In this study, the nonlinear relationship between circuit parameters and SOC is explicitly characterized using analytical polynomial functions. The effect of polynomial order is systematically investigated by means of fitting and prediction accuracy, in which the prediction performance is evaluated using leave-one-out cross-validation (LOOCV) method. The EIS measurements of a 20-A·h commercial LIB are performed to demonstrate the effectiveness of the proposed model. The results show that a seventh-order polynomial function is sufficiently high to capture the nonlinear effect of SOC on circuit parameters. Moreover, the LOOCV prediction performance of the polynomial function-based ECM is probably better than that of a common interpolation-based ECM.**

***Index Terms*—Electrochemical impedance spectroscopy (EIS), equivalent circuit model (ECM), lithium-ion batteries (LIB), polynomial function, state of charge (SOC).**

## I. Introduction

LITHIUM-ION batteries (LIBs), as a promising type of energy storage devices, have been increasingly used in a wide range of applications, such as portable electronic devices, electric vehicles, and hybrid electric vehicles [1]–[4]. In general, successful commercialization of LIBs often requires a high-fidelity battery management system (BMS) to guarantee safe, efficient, and reliable operations of LIBs [5]–[7]. As two key functions of BMS, both state of charge (SOC) estimation [8]–[10] and state of health (SOH) prognostics [11], [12] have attracted growing attention. Since both SOC and SOH cannot be measured directly, a combined strategy of the mathematical model and the state estimation method is often applied to perform SOC estimation and SOH prognostics [13]. Among the measurement techniques that have been employed to assist in constructing mathematical model, electrochemical impedance spectroscopy (EIS) provide a promising tool to study electrochemical reaction kinetics and transport mechanisms in LIBs [14], [15]. Although EIS could be in nature suitable for accurate SOC estimation and SOH prognostics [16]–[18], its online implementation in BMS is scarce due to relatively strict measurement condition and high cost. Moreover, the nonlinear relationship between EIS data and SOC is rarely modeled on a quantitative basis and thus needs to be further investigated.

EIS data are usually interpreted using equivalent circuit models (ECMs), which typically consist of inductance, resistance, capacitance, constant phase element (CPE), and Warburg element. Generally, different combinations of elements result in different ECMs, which can describe various impedance characteristics such as ion conduction, diffusion and migration, charge transfer, and solid-state ion diffusion [19]. In the past decades, diverse ECMs have been proposed to elucidate the reaction and transport mechanisms not only in electrodes [20], [21], but also in full cells [14], [22]. It has been recognized that the same impedance spectrum might be nicely fitted by several different ECMs [19]. It is often difficult to determine a proper structure of ECM to model EIS data without a clear understanding of the complicated electrochemical process. If analyzing EIS data from a commercial battery, separation of the parameters corresponding to the positive and negative electrodes would become more difficult, as the individual electrode parameters are almost comparable in magnitudes [23]. Although such parameters separation might be tackled through proper assumptions, its validity needs to be further investigated [23]. From the viewpoint of SOC estimation and SOH prognostics by means of EIS measurements, one of the most important tasks is to extract one or several key impedance parameters, which should be sensitive to SOC and SOH variations. Hence, this study is mainly focused on constructing a suitable ECM to interpret EIS data of a commercial battery, while neglecting separating the individual electrode parameters to some extent. However, both fitting and

Manuscript received June 17, 2017; revised September 28, 2017 and November 13, 2017; accepted November 29, 2017. Date of publication December 6, 2017; date of current version July 15, 2018. This work was supported in part by the National Key R&D Program of China under Grant 2016YFB0901500, in part by the National Natural Science Foundation of China under Grant 21576163, and in part by the Science and Technology Commission of Shanghai Municipality under Grant 14DZ2250800. Recommended for publication by Associate Editor F. H. Khan. *(Corresponding authors: Yi-Jun He and Xiao-Song Hu.)*

Q.-K. Wang, Y.-J. He, J.-N. Shen, and Z.-F. Ma are with the Department of Chemical Engineering, Shanghai Electrochemical Energy Devices Research Center, Shanghai Jiao Tong University, Shanghai 200240, China (e-mail: wqkyy@sjtu.edu.cn; heyijun@sjtu.edu.cn; jennyshen@sjtu.edu.cn; zfma@sjtu.edu.cn).

X.-S. Hu is with the Department of Automotive Engineering, Chongqing University, Chongqing 400044, China (e-mail: xiaosonghu@ieee.org).

Color versions of one or more of the figures in this paper are available online at http://ieeexplore.ieee.org.

Digital Object Identifier 10.1109/TPEL.2017.2780184

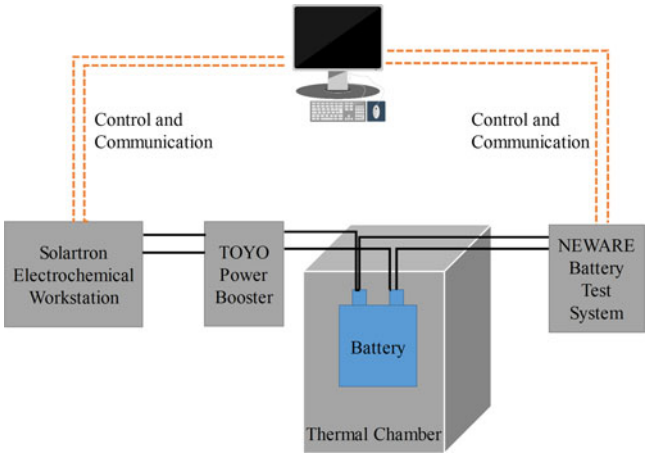


Fig. 1. Schematic diagram of the battery test bench.

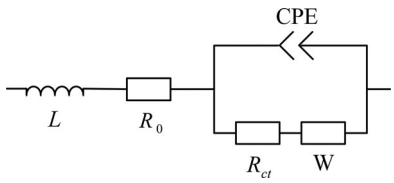


Fig. 2. Equivalent circuit used to model impedance spectra.

prediction performance of ECM should be properly evaluated to determine a compact, simple, yet accurate ECM.

It is well known that the circuit parameters are dependent on SOC and temperature [22], [24]–[27]. While the impacts of SOC and temperature on circuit parameters have been widely investigated, most studies focus on mechanism interpretation and are in nature only qualitative [22], [25]. Traditionally, each ECM is individually constructed based on one EIS spectrum at a specific SOC and temperature. Recently, the nonlinear quantitative relationship between circuit parameters and SOC/temperature has been studied using empirical equations such as polynomial functions or exponential functions [24], [28]. However, the fitting performance is only examined based on correlation coefficient criterion. Consequently, the prediction performance might not be guaranteed in practical applications [24].

The salient original contribution of this paper delivered to the related literature is as follows: the leave-one-out cross-validation (LOOCV) method is leveraged to assess the prediction performance of the ECM and consequently to assist in optimally selecting the polynomial order for each SOC-dependent circuit parameter. To the best of our knowledge, this study is the first attempt to propose an explicit SOC-embedded polynomial ECM for interpreting EIS data at various SOC values, with a systematic evaluation of model sensitivity to the polynomial order.

The remainder of this paper is structured as follows. The EIS experimental setup is introduced in Section II. The traditional interpolation-based ECM, the polynomial ECM, and the parameter estimation strategy are then described in Section III. The fitting and prediction performance of both interpolation and polynomial ECMs is assessed in Section IV. Finally, main concluding remarks are presented in Section V.

## II. Experimental Setup

A commercial pouch-type $LiFePO_4$ battery with a nominal capacity of 20 A·h and voltage of 3.2 V was used in this experiment. The schematic diagram of the battery test bench is shown in Fig. 1. The EIS measurements were conducted at various temperatures and SOC values using a Solartron 1287 Electrochemical Interface, TOYO power booster PBi250-10, and a 1260 impedance/gain-phase analyzer controlled by Zplot and Corrware software. The EIS measurements were performed in the frequency range from 1 kHz to 10 mHz and at a voltage amplitude of 10 mV. Numerous SOC values between 0% and 100% were obtained with a NEWARE Model CT-4008-5V10A-FA battery test system, and the temperature range from 273 to 303 K were achieved using a JIWEI Model GD4010 programmable temperature test chamber.

Before measuring EIS data, the usable capacity of battery was calibrated by a standard reference capacity test method. First, the battery was charged by the constant current and constant voltage (CCCV) method. Then, the battery was discharged using constant current (CC) of 7 A to the cut-off voltage of 2.5 V. Finally, both CCCV charge and CC discharge tests was repeated for three times, and the average of three discharge capacity values is calculated as the battery usable capacity. In this study, after raising or lowering the cell ambient temperature to the target value, a soak period of 2 h was permitted for thermal equalization before the EIS measurement. First, the cell was charged using a CC of 7 A until the voltage reached to the cut-off voltage of 3.65 V and then charged at constant voltage of 3.65 V until the current decayed to 0.4 A. Then, the cell was discharged using a CC of 7 A to a specific SOC step by step, and then the EIS measurement was carried out at each SOC step. Finally, repeat the previous two steps for each specified temperature for obtaining all impedance spectra.

## III. Methodology

### A. ECM

An equivalent circuit is proposed to model impedance spectra as shown in Fig. 2, in which $L$, $R_0$, $R_{\rm ct}$, W, and CPE denote inductance, ohmic resistance, charge transfer resistance, Warburg impedance, and CPE, respectively. The inductance component originates from the porosity of electrode and connection leads to the battery at high frequencies, and the complex impedance of inductance component $Z_L$ is defined as

$$Z_L = j\omega L \tag{1}$$

where $\omega$ is the angular frequency of ac signal. The ohmic resistance component includes the electrolyte resistance, contact resistance, electronic contacts, etc. The charge transfer resistance component mainly arises from the charge transfer in the solid electrolyte interface (SEI) layer of the electrode and the electrode/electrolyte interface. The impedances of ohmic resistance component $Z_{R_0}$ and charge transfer resistance component

$Z_{R_{\rm ct}}$ are simply defined as

$$Z_{R_0} = R_0 \tag{2}$$

$$Z_{R_{\rm ct}} = R_{\rm ct}. \tag{3}$$

The CPE component is used to model the behavior of imperfect dielectrics, and the complex impedance of CPE $Z_{\rm CPE}$ is described by [29]

$$Z_{\rm CPE} = \frac{1}{(j\omega)^n Q} \tag{4}$$

where $Q$ is the time constant, and $n$ is a real number between 0 and 1. When $n = 0$, it corresponds to a pure resistor, and when $n = 1$ to a pure capacitor. The generalized finite-length Warburg element is used to model the solid-state lithium-ion diffusion process [15], [20], [30], and the complex impedance of Warburg component $Z_W$ is given by [30]

$$Z_W = R_W \frac{\tanh(j\omega\tau)^\phi}{(j\omega\tau)^\phi} \tag{5}$$

where $\tau$ is the diffusion time constant, $\phi$ varies between 0 and 1, and $R_W$ is the Warburg resistance. The overall impedance of the equivalent circuit in Fig. 2 can be formulated as

$$Z_{\rm ECM} = Z_L + Z_{R_0} + \frac{1}{\frac{1}{Z_{\rm CPE}} + \frac{1}{Z_{R_{ct}} + Z_W}}. \tag{6}$$

Based on the description above, there are eight circuit parameters in the ECM to estimate, which can be described as $\boldsymbol{\beta} = [L, R_0, R_{\rm ct}, Q, n, R_W, \tau, \phi]^T$. A complex nonlinear least-squares (CNLS) method was used to fit EIS data based on the equivalent circuit in Fig. 2. CNLS will minimize a weighted sum of squares error (*WSSE*) of the difference between the experimental and calculated impedances, which is defined as

$$WSSE = \sum_{k=1}^{K} \Big\{ w'_k [Z'_{\rm exp}(\omega_k) - Z'_{\rm calc}(\omega_k, \boldsymbol{\beta})]^2 + w''_k [Z''_{\rm exp}(\omega_k) - Z''_{\rm calc}(\omega_k, \boldsymbol{\beta})]^2 \Big\} \tag{7}$$

where $K$ is the number of frequencies, $w'_k$ and $w''_k$ are the weights of data points, $Z'_{\rm exp}(\omega_k)$ and $Z''_{\rm exp}(\omega_k)$ are the real and imaginary parts of the experimental impedances at $\omega_k$, respectively, and $Z'_{\rm calc}(\omega_k, \boldsymbol{\beta})$ and $Z''_{\rm calc}(\omega_k, \boldsymbol{\beta})$ are the real and imaginary parts of the calculated impedances at $\omega_k$, respectively. In this study, a modulus weighting strategy is adopted to guarantee that small and large impedances take an equal contribution to the sum of squares. Hence, both $w'_k$ and $w''_k$ are set equal to $1/\|Z_{\rm exp}(\omega_k)\|^2 = 1/\{[Z'_{\rm exp}(\omega_k)]^2 + [Z''_{\rm exp}(\omega_k)]^2\}$.

### *B. Polynomial ECM and Parameter Estimation*

Since both SOC and temperature influence impedance spectra, the circuit parameters are often estimated for each specified SOC and temperature. Then, the interpolation method can be introduced to estimate the circuit parameters at unseen SOC and temperature. However, in this study, the circuit parameters $\boldsymbol{\beta}$ are explicitly modeled as polynomial functions of SOC, which are represented as

$$\boldsymbol{\beta}_i = \sum_{j=0}^{N} \boldsymbol{\alpha}_{ij} {\rm SOC}^j, \quad i = 1, \ldots, 8 \tag{8}$$

where $N$ is the order of polynomial function and $\boldsymbol{\alpha}_i$ is polynomial coefficients of the $i$th circuit parameters in $\boldsymbol{\beta}$. *SOC* is estimated by the Coulomb counting method with relatively high accurate current measurement in the laboratory, which is calculated by

$${\rm SOC} = 1 - \frac{\int_0^t I dt}{C_n} \tag{9}$$

where $C_n$ is the discharge capacity calibrated by a standard reference capacity test method. Thus, there are total $8(N + 1)$ parameters to estimate. Note that these circuit parameters should be larger than 0 to ensure their physical meaningful. Hence, the parameter estimation problem can be summarized as

$$\min \sum_{p=1}^{P} WSSE_p \tag{10}$$

s.t. Constraints (8)

$$\boldsymbol{\beta}_i = \sum_{j=0}^{N} \boldsymbol{\alpha}_{ij} {\rm SOC}^j > 0, \quad i = 1, \ldots, 8 \tag{11}$$

where $P$ is the number of experimental impedance spectra corresponding to different SOC values. The CNLS problems are solved by fmincon with the trust-region-reflective algorithm in MATLAB optimization toolbox.

### *C. Model Performance Evaluation Criteria*

To evaluate the fitting and prediction performance of the established ECM on one impedance spectrum, two criteria, namely the root mean square error (RMSE) and mean absolute percentage error (MAPE), are used, which are defined as follows:

$${\rm RMSE} = \sqrt{\frac{\sum_{k=1}^{K} \Big\{ [Z'_{\rm exp}(\omega_k) - Z'_{\rm calc}(\omega_k, \boldsymbol{\beta}^*)]^2 + [Z''_{\rm exp}(\omega_k) - Z''_{\rm calc}(\omega_k, \boldsymbol{\beta}^*)]^2 \Big\}}{2K}} \tag{12}$$

$${\rm MAPE}(\%) = \frac{100}{2K} \sum_{k=1}^{K} \left[ \left| \frac{Z'_{\rm exp}(\omega_k) - Z'_{\rm calc}(\omega_k, \boldsymbol{\beta}^*)}{Z'_{\rm exp}(\omega_k)} \right| + \left| \frac{Z''_{\rm exp}(\omega_k) - Z''_{\rm calc}(\omega_k, \boldsymbol{\beta}^*)}{Z''_{\rm exp}(\omega_k)} \right| \right] \tag{13}$$

where $\boldsymbol{\beta}^*$ is the optimal parameters estimated by solving the CNLS problems. Since both (12) and (13) are only used for one impedance spectrum, the average values of RMSE and MAPE should be computed for a set of impedance spectra with different temperatures and SOC values. For the ease of description, AFRMSE and AFMAPE are introduced to represent the average fitting RMSE and MAPE for all SOC values at a specific

temperature, and are defined as follows:

$$\mathrm{AFRMSE} = \frac{1}{P}\sum_{p=1}^{P}\mathrm{RMSE}_p \tag{14}$$

$$\mathrm{AFMAPE} = \frac{1}{P}\sum_{p=1}^{P}\mathrm{MAPE}_p. \tag{15}$$

In the proposed polynomial ECM, the order of polynomial functions should be optimally determined. Although various statistical testing methods such as chi-square, *F*-test and *t*-test have been proposed to guide the optimal selection of model structure, these indicators might be not sufficient to determine the goodness of fit [31]. Note that these statistical testing methods only focus on the fitting residuals and may not guarantee a good prediction performance on the unseen data points. Cross-validation method is a promising model evaluation method, in which the whole experimental dataset is first divided into training set and testing set, then the model is constructed in terms of training set, and finally the model is independently evaluated in terms of testing set. In this work, a particular cross-validation method, namely LOOCV [32], is used to assess the prediction performance of the polynomial ECM and guide the selection of the polynomial order. In the LOOCV method, at each time, one of *P* sets of experimental impedance spectra is selected as testing spectrum, and the remaining *P*–1 spectra are used to establish the polynomial ECM. There are total *P* runs of model construction, and the average prediction performance can be evaluated on the *P* sets of testing spectra. Two experimental impedance spectra corresponding to 0% and 100% SOC are always kept in training spectra. Hence, at each temperature, there are total *P*–2 runs for performing cross validation. Two more criteria, namely APRMSE and APMAPE, are defined to represent the LOOCV average prediction RMSE and MAPE, respectively

$$\mathrm{APRMSE} = \frac{1}{P-2}\sum_{p=2}^{P-1}\mathrm{RMSE}_p \tag{16}$$

$$\mathrm{APMAPE} = \frac{1}{P-2}\sum_{p=2}^{P-1}\mathrm{MAPE}_p. \tag{17}$$

Given a set of *P* EIS spectra with $\mathrm{SOC}_p$ ($p = 1, 2, \ldots, P$) at a specific temperature, the implementation of the LOOCV method for selecting optimal polynomial order can be briefly described as follows. Note that the EIS spectra with 0% and 100% SOC corresponding to the *p* values of 1 and *P*, respectively, are excluded to be testing spectra.

*Step 1:* Set $N = 1$, where *N* denotes the order of polynomial;
*Step 2:* Set $p = 2$, where *p* denotes the index of EIS spectra;
*Step 3:* Set the testing set as the EIS spectra with $\mathrm{SOC}_p$, and set the training set as the EIS spectra with other *SOC* values;
*Step 4:* Construct the *N*th-order polynomial ECM using the training set;
*Step 5:* Compute the prediction $\mathrm{RMSE}_p$ and $\mathrm{MAPE}_p$ values for the *p*th testing set based on (12) and (13), respectively;

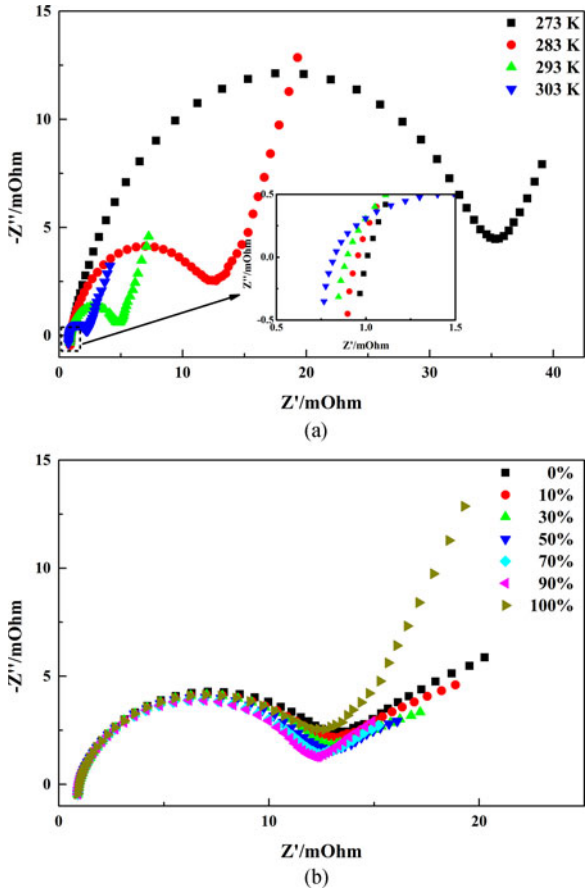


Fig. 3. Nyquist plots of a 20-A·h LiFePO4 battery: (a) temperature effect at 100% SOC and (b) SOC effect at 283 K.

*Step 6:* Set $p = p + 1$; if *p* is less than *P*, then go to Step 3; otherwise, go to Step 7;
*Step 7:* Calculate the $\mathrm{APRMSE}_N$ and $\mathrm{APMAPE}_N$ values for the *N*th-order polynomial ECM based on (16) and (17), respectively;
*Step 8:* Set $N = N + 1$; if *N* is no more than $N_{\max}$ (the prescribed maximal polynomial order), then go to Step 2; otherwise, go to Step 9;
*Step 9:* Determine the optimal polynomial order corresponding to minimal APRMSE or APMAPE.

## IV. Results and Discussion

### A. Impedance Response of LIBs

Fig. 3(a) and (b) shows the effects of temperature and SOC on Nyquist impedance spectra at a SOC of 100% and a temperature of 283 K for a commercial 20 A·h $\mathrm{LiFePO_4}$ battery, respectively. $Z'$ and $Z''$ in Fig. 3 are the real and imaginary impedance responses of the battery, respectively. It can be apparently seen from Fig. 3 that all the impedance spectra are composed of an inductive tail at high frequencies, a depressed semicircle at medium frequencies, and a straight slope line at low frequencies. In general, the porosity of the electrode and connection leads to the battery result in the inductance

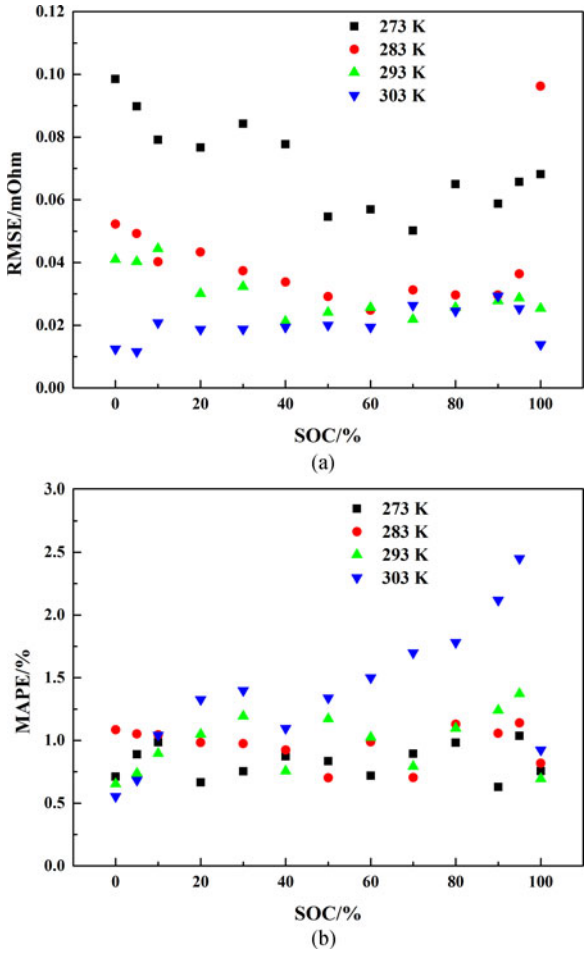


Fig. 4. Fitting performance of the traditional ECM at different temperatures and SOC: (a) RMSE and (b) MAPE.

phenomenon [28], the depressed semicircle at medium frequencies originates from the SEI layer of the electrode and electrode/electrolyte interface, and the straight line represents the solid-state lithium-ion diffusion into the porous electrode matrix [24]. From Fig. 3(a), it is observed that the semicircle becomes more depressed as temperature increases. It is mainly ascribed to the fact that the charge transfer rate in the SEI layer and electrode/electrolyte interface increases at higher temperature. From the enlarged view in Fig. 3(a), the total ohmic resistance, represented by the high-frequency intercept on the real axis, decreases as temperature increases. That might be explained by an increased ion transfer rate in the electrolyte solution at higher temperature.

Compared with the impact of temperature on impedance spectra in Fig. 3(a), the impact of SOC on impedance spectra shown in Fig. 3(b) is relatively less significant. However, it can be observed that the SOC mainly influences the charge transfer rate in the medium-frequency range and the solid-state lithium-ion diffusion rate in the low-frequency range, while the total ohmic resistances at the high-frequency intercept on the real axis are almost the same in the whole SOC range. As the SOC increases from 0% to 90%, the semicircle shows a slight depressed, and the

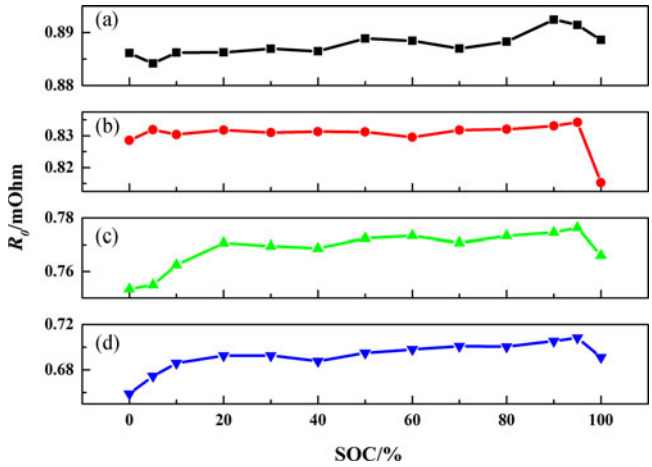


Fig. 5. Ohmic resistance profiles with respect to SOC at different temperatures: (a) 273 K, (b) 283 K, (c) 293 K, and (d) 303 K.

slope line decreases in both the real and imaginary directions, while at the SOC of 100%, the slope line shows a significant increase in both the real and imaginary directions. However, it should be noted that the impact of SOC on impedance spectra would be dissimilar at different temperatures, and the impact of temperature on impedance spectra would be varied at different SOC values.

### *B. Fitting Performance Evaluation of Traditional ECM*

The ECM shown in Fig. 2 is used to model impedance spectra. Before evaluating the effectiveness of the proposed polynomial ECM method, ECMs are first separately established for each SOC and temperature. Fig. 4(a) and (b) shows the fitting RMSE and MAPE at different temperatures and SOC values, respectively. It is found that the maximal fitting RMSE and MAPE are less than 0.1 mΩ and 2.5%, respectively, and the average fitting RMSE and MAPE for all 52 impedance spectra are 0.04 mΩ and 1.04%, respectively. These small fitting errors indicate that the equivalent circuit in Fig. 2 is complex enough to capture the nonlinear behavior of the impedance spectra.

### *C. Effects of SOC and Temperature on Circuit Parameters*

The impacts of temperature and SOC on the circuit parameters are thoroughly investigated. Figs. 5, 6, and 7 show the effects of temperature and SOC on the ohmic resistance, charge transfer resistance, and Warburg resistance, respectively. It is found from Fig. 5 that the ohmic resistance decreases with the increase in temperature, i.e., the average ohmic resistances for all SOC values are 0.89, 0.83, 0.77, and 0.69 mΩ at temperatures of 273, 283, 293, and 303 K, respectively. This is in accordance with the phenomenon that the intercept on the real axis at high frequencies decreases as the temperature increases, as shown in Fig. 3(a). It is clearly observed that the ohmic resistance shows less significant dependence on SOC than on temperature. The ohmic resistance remains almost constant with small fluctuations in the SOC range of [0%, 95%] at temperatures of 273 and 283 K, while at the temperatures of 293 and 303 K, the ohmic

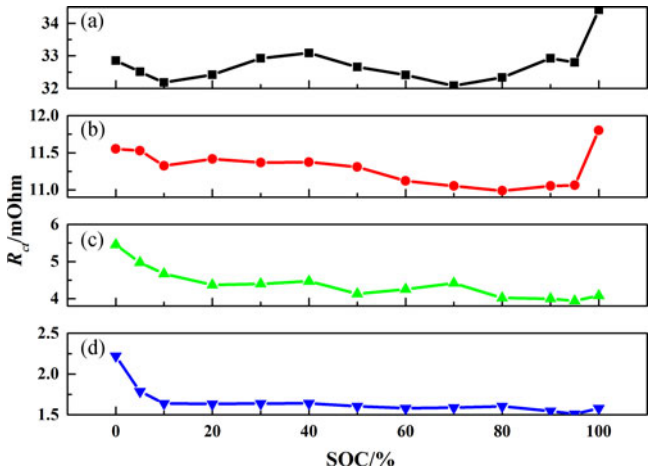


Fig. 6. Charge transfer resistance profiles with respect to SOC at different temperatures: (a) 273 K, (b) 283 K, (c) 293 K, and (d) 303 K.

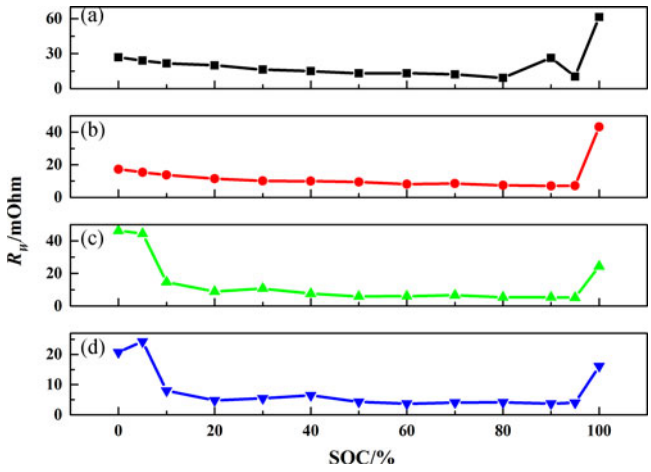


Fig. 7. Warburg resistance profiles with respect to SOC at different temperatures: (a) 273 K, (b) 283 K, (c) 293 K, and (d) 303 K.

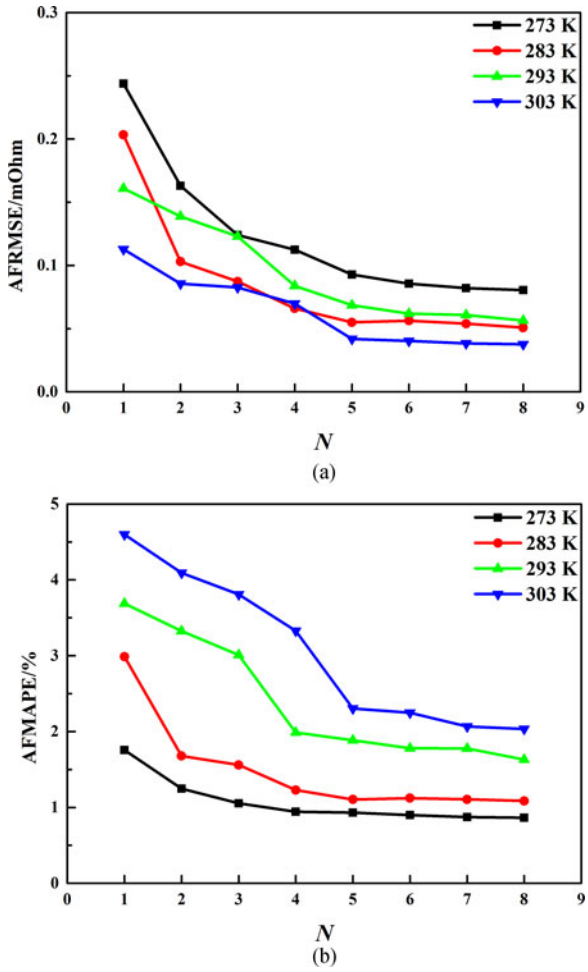


Fig. 8. Fitting performance criteria profiles with respect to polynomial order at different temperatures: (a) AFRMSE and (b) AFMAPE.

resistance first increases as SOC increases from 0% to 20%, and then keeps almost constant in the SOC range of [20%, 95%]. Meanwhile, the ohmic resistance shows a small decrease trend at all temperatures, when SOC increases from 95% to 100%.

From Fig. 6, it can be seen that the charge transfer resistance displays a significant decrease, as the temperature increases, namely, the average charge transfer resistance significantly decreases from 32.7 to 1.66 mΩ, as the temperature increases from 273 to 303 K. Compared to Fig. 5, it is noted that the impact of temperature on the charge transfer resistance is more significant than on ohmic resistance. The charge transfer resistance fluctuates in a small range in the whole SOC range at each temperature, i.e., 32.1–34.4 mΩ at 273 K, 11.0–11.8 mΩ at 283 K, 3.9–5.5 mΩ at 293 K, and 1.5–2.2 mΩ at 303 K. Therefore, it implies that similar to the ohmic resistance, the charge transfer resistance also shows less significant dependence on SOC than on temperature.

Fig. 7 illustrates the Warburg resistance variations with SOC at different temperatures. In the SOC range of [10%, 95%], the Warburg resistance usually decreases with the increase in temperature. In the lowest SOC range of [0%, 5%], the Warburg resistance shows a sudden increase trend at relatively high temperatures of 293 and 303 K, and in the highest SOC range of [95%, 100%], a sudden increase trend is observed at all temperatures. The possible reason is that the accumulation of lithium ions in the positive/negative electrodes during the discharge/charge processes would significantly decrease the solid-state lithium-ion diffusion rate, especially in the situations with extremely low and high SOC, and consequently lead to the increase of the Warburg resistance. It is reasonable to conclude from Figs. 5, 6, and 7 that both charge transfer and Warburg resistances show a comparable order of magnitude at each temperature and are much larger than the ohmic resistance. In addition, SOC plays a larger impact on the Warburg resistance than on both ohmic and charge transfer resistances.

### *D. Fitting Performance Evaluation of Polynomial ECM*

The proposed polynomial ECM is used to model impedance spectra for all SOC values at each temperature. The effect of polynomial order, varying from 1 to 8, on fitting performance is

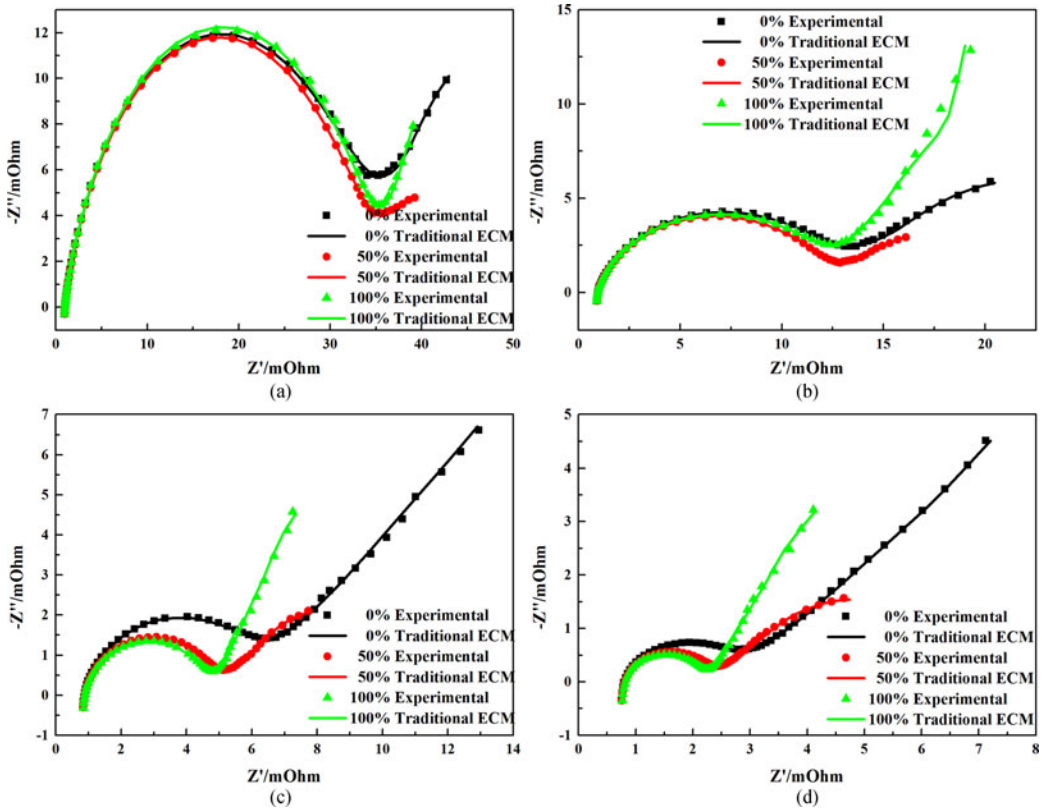


Fig. 9. Fitted impedance data using traditional ECM at different SOC and temperatures: (a) 273 K, (b) 283 K, (c) 293 K, and (d) 303 K.

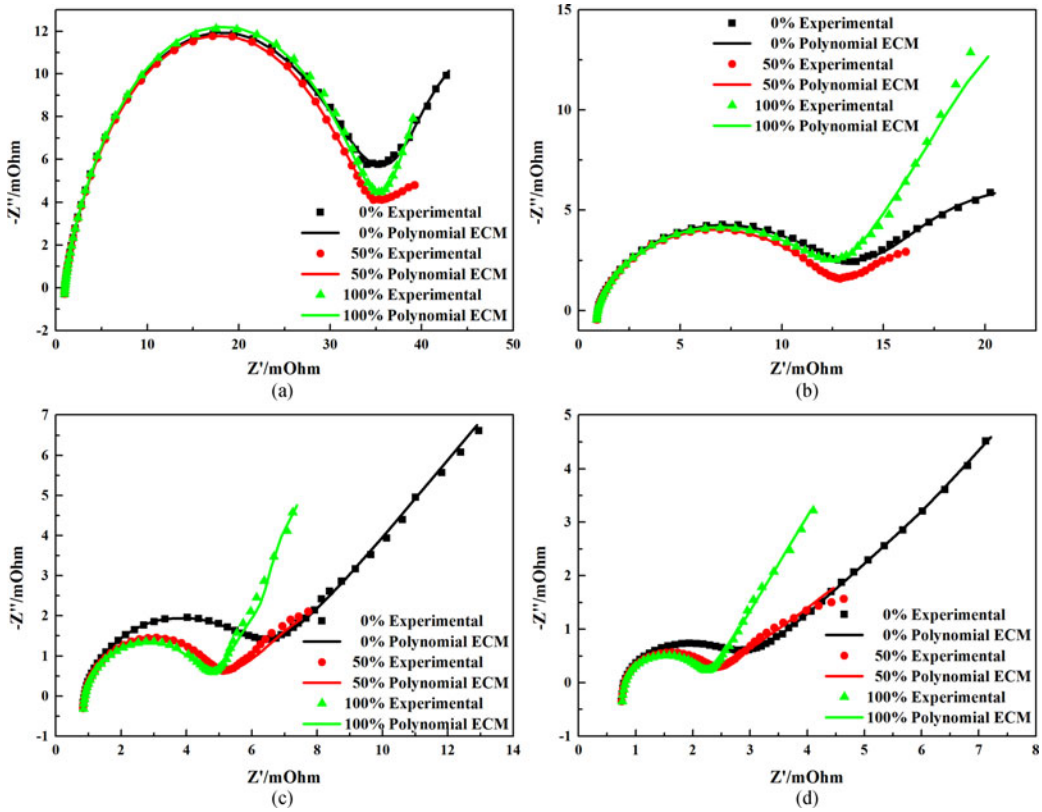


Fig. 10. Fitted impedance data using seventh-order polynomial ECM at different SOC and temperatures: (a) 273 K, (b) 283 K, (c) 293 K, and (d) 303 K.

thoroughly investigated. Note that the computational cost of offline parameter estimation generally increases with the increase of polynomial order. For example, the parameters estimation for the first-order polynomial ECM can be completed in 5 h, while the computational time would increase to 12 h for the eighth-order polynomial ECM. However, it should be also noted that the computational cost could be significantly reduced, given relatively proper initial guesses of parameters. Fig. 8(a) and (b) shows AFRMSE and AFMAPE variations with polynomial order at different temperatures, respectively. It is clear that both AFRMSE and AFMAPE usually decrease with the increasing of the polynomial order. After increasing the polynomial order above 5, both AFRMSE and AFMAPE are kept almost constant. It implies that the polynomial order of 5 is sufficiently high enough to capture the nonlinear relationship between SOC and circuit parameters of this commercial 20-A·h LIB, from the viewpoint of fitting performance evaluation. However, it is worth noting that since the relationships between SOC and different circuit parameters might show different complexities, separately selecting the optimal polynomial order for each parameter could be an interesting research direction.

From Fig. 8(a) and (b), it is discerned that: 1) the AFRMSE values of the eighth-order polynomial ECM are 0.08, 0.05, 0.06, and 0.04 mΩ at the temperatures of 273, 283, 293, and 303 K, respectively; and 2) the AFMAPE values of the eighth-order polynomial ECM are 0.86%, 1.09%, 1.63%, and 2.03% at the temperatures of 273, 283, 293, and 303 K, respectively. Moreover, the average AFRAMSE and AFMAPE are calculated to be 0.06 mΩ and 1.40% for all 52 impedance spectra, respectively, which are almost the same as the average RMSE and MAPE of 0.04 mΩ and 1.04% for the separately established ECM. It underlines that a polynomial function can be effectively applied to capture the nonlinear relationship between SOC and circuit parameters, which would improve the flexibility of ECM, when it is used to predict other impedance spectra, as well as circuit parameters at different SOC values.

To illustrate whether the established ECMs could finely fit the experimental impedance spectra, Figs. 9 and 10 show the fitted impedance data using the traditional ECM and the seventh-order polynomial ECM at different SOC values and temperatures, respectively. It is observed that both models show good agreement with the experimental impedance spectra over a wide range of frequencies, SOC, and temperatures. Moreover, as compared to the traditional ECM, the polynomial ECM almost shows a comparable fitting performance. It further validates the effectiveness of the proposed polynomial ECM, which is ready for predicting the impedance spectra and circuit parameters at other unseen SOC. However, it is worth noting that the selection of polynomial order should be dependent not only on fitting performance but also on prediction performance, and we will use LOOCV prediction performance criteria to determine the polynomial order in the following section.

### *E. LOOCV Prediction Performance Evaluation of Polynomial ECM*

To evaluate the prediction performance of the proposed polynomial ECM and guide the selection of polynomial order, the

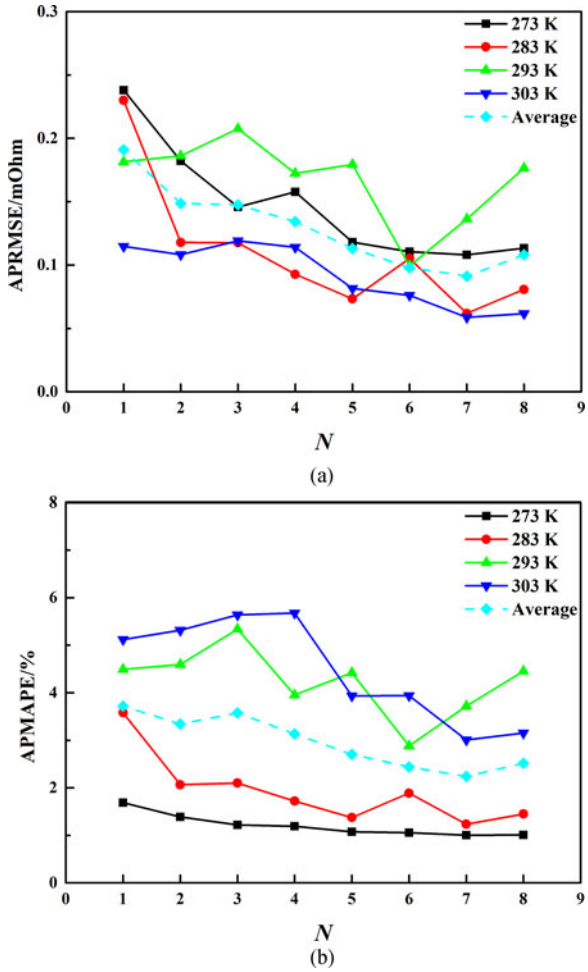


Fig. 11. Leave-one-out prediction performance criteria profiles with respect to polynomial order: (a) APRMSE and (b) APMAPE.

LOOCV prediction APRMSE and APMAPE variations with a range of polynomial orders are shown in Fig. 11(a) and (b), respectively. It is obvious that: 1) both APRMSE and APMAPE values mostly decrease, as the polynomial order increases at relatively low temperatures of 273 and 283 K; 2) both of them show significant fluctuations at the temperatures of 293 K; and 3) at relatively high temperature of 303 K, the prediction performance criteria first show a slight deterioration, as the polynomial order increases from 1 to 4, and then decrease, as the polynomial order increases from 4 to 8.

Note that the fitting performance often improves, as the model complexity increases, while the prediction performance usually first improves with the increasing of the model complexity and then becomes degraded as the model complexity further increases. Since the model complexity is represented by the polynomial order in this study, a proper selection of the polynomial order should simultaneously consider the fitting and prediction performance. It is found that the minimal values of APRMSE are 0.11, 0.06, 0.10, and 0.06 mΩ at temperatures of 273, 283, 293, and 303 K, respectively, which are corresponding to the seventh-, seventh-, sixth-, and seventh-order polynomial ECMs, respectively. The minimal values of APMAPE are 1.00%, 1.23%, 2.88%, and 3.01% at temperatures of 273, 283,

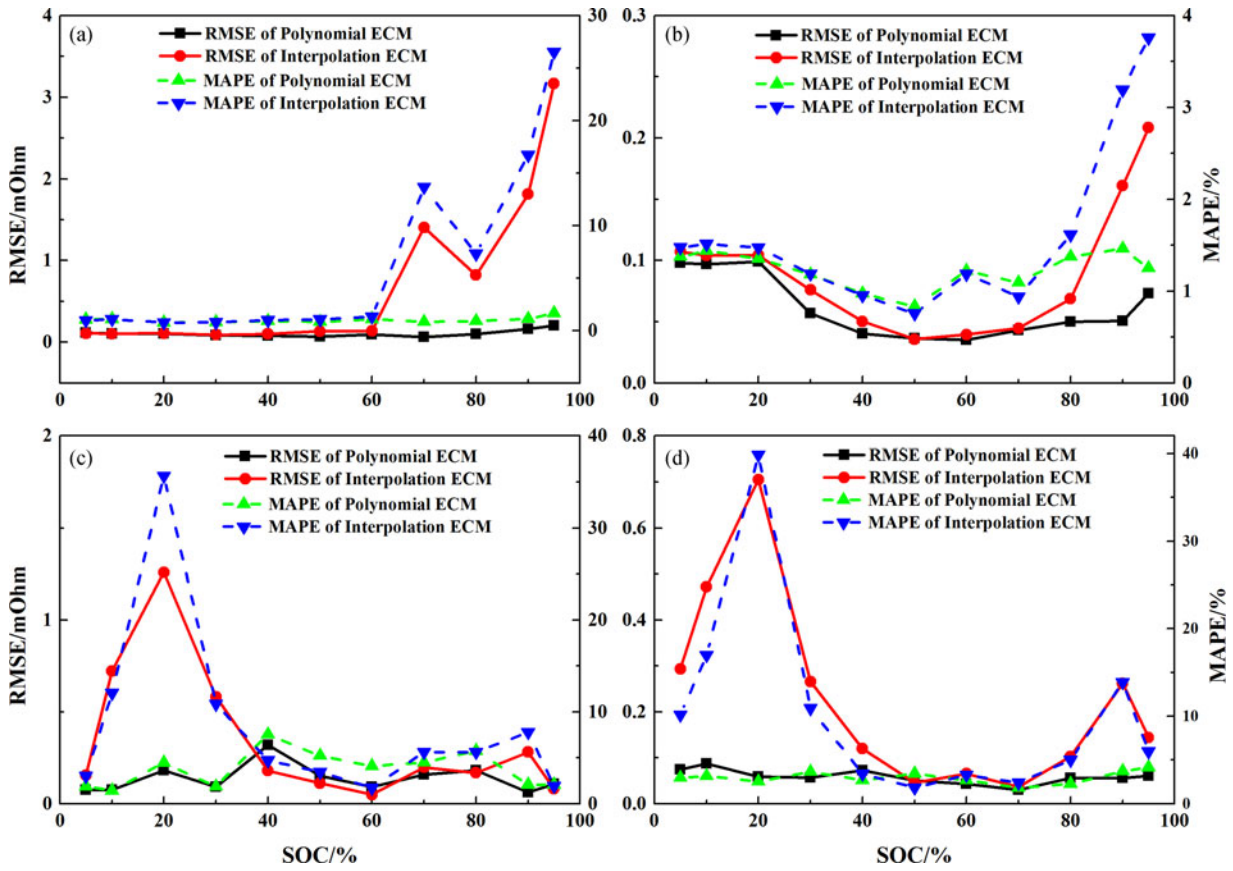


Fig. 12. Leave-one-out prediction performance comparisons between polynomial ECM and interpolation ECM at different SOC and temperatures: (a) 273 K, (b) 283 K, (c) 293 K, and (d) 303 K.

293, and 303 K, respectively. Similarly, the polynomial order corresponding to the minimal APMAPE value is the same as that of APRMSE at each temperature. Moreover, it is found from Fig. 11 that the average values of APRMSE and APMAPE for all temperatures have the minimal values of 0.09 mΩ and 2.24% using the seventh-order polynomial ECMs. In addition, as illustrated in Fig. 7, a polynomial order of 5 is high enough to give a good fitting performance. Hence, it is reasonable to determine the optimal polynomial order to be 7, in terms of both fitting and LOOCV prediction performance.

### *F. Prediction Performance Comparison*

To further demonstrate the effectiveness of the proposed polynomial ECM, the LOOCV prediction performance of the seventh-order polynomial ECM is compared with that of an interpolation-based ECM method, in which a cubic spline method is used to predict the circuit parameters in a LOOCV manner. Fig. 12(a), (b), (c), and (d) shows the LOOCV prediction RMSE and MAPE variations with SOC using the polynomial ECM and interpolation ECM at the temperatures of 273, 283, 293, and 303 K, respectively.

As shown in Fig. 12(a)–(d), it is found that for the polynomial ECM, the maximal values of RMSE are less than 0.20, 0.10, 0.32, and 0.09 mΩ for all SOC values at temperatures of 273, 283, 293, and 303 K, respectively, while the maximal RMSE values of the interpolation ECM can reach 3.17, 0.21, 1.26, and 0.71 mΩ at temperatures of 273, 283, 293, and 303 K, respectively. Likewise, the maximal MAPE values of the polynomial ECM are less than 1.65%, 1.46%, 7.54%, and 4.17% at temperatures of 273, 283, 293, and 303 K, respectively, while for the interpolation ECM, the maximal MAPE values are 26.54%, 3.76%, 35.67%, and 39.87% at temperatures of 273, 283, 293, and 303 K, respectively. Moreover, it can be easily observed that the interpolation ECM shows large prediction errors in the relatively high SOC range of [80%, 95%] at 273 K, in the high SOC range of [80%, 95%] at 283 K, in the low SOC range of [10%, 40%] at 293 K, and in both low SOC range of [5%, 40%] and high SOC range of [80%, 95%] at 303 K. It implies that the interpolation method would fail to predict proper circuit parameters in some SOC ranges at different temperatures. On the other hand, the polynomial ECM shows small prediction errors with narrow fluctuations in terms of RMSE and MAPE over a wide range of SOC and temperature. It is reasonable to conclude that the proposed polynomial ECM can effectively capture the nonlinear relationship between SOC and circuit parameters and is suitable to perform reliable and accurate predictions of circuit parameters with unseen SOC values. In addition, compared with the interpolation ECM, the superiority of the polynomial ECM is again validated.

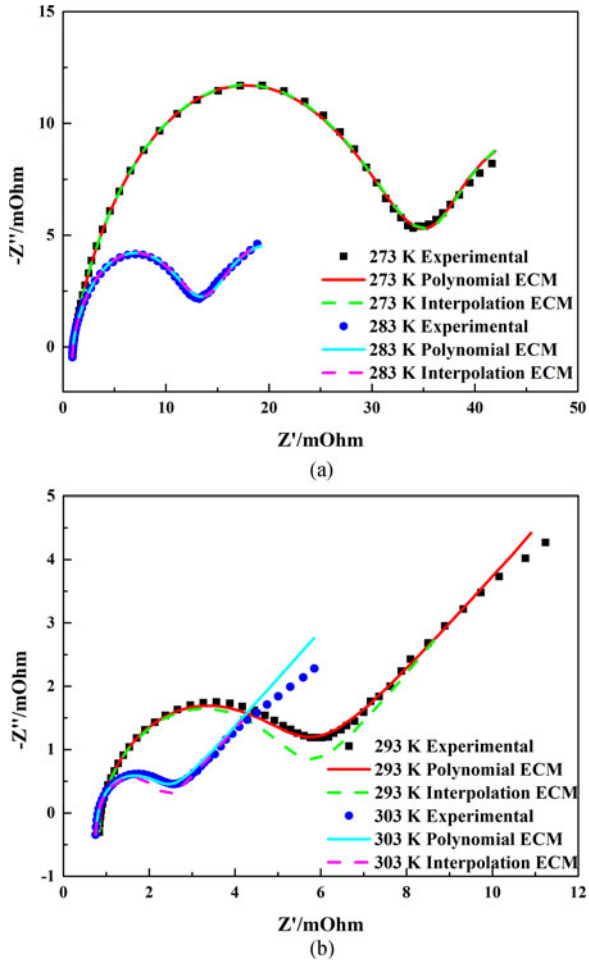


Fig. 13. Predicted impedance spectra with 10% SOC using the polynomial ECM and interpolation ECM at different temperatures.

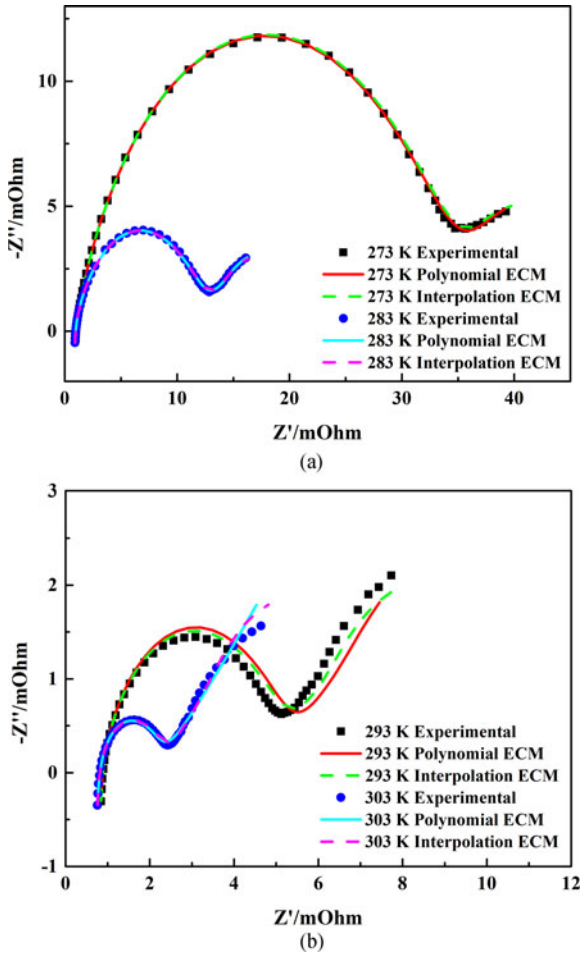


Fig. 14. Predicted impedance spectra with 50% SOC using the polynomial ECM and interpolation ECM at different temperatures.

Figs. 13, 14, and 15 shows the predicted impedance spectra using the polynomial ECM and interpolation ECM at 10%, 50%, and 90% SOC, respectively. From Fig. 13, it is found that: 1) at relatively low temperatures of 273 and 283 K, the predicted impedance spectra of both polynomial ECM and interpolation ECM almost coincide with the experimental impedance spectra over the whole range of frequencies; and 2) at relatively high temperatures of 293 and 303 K, the interpolation ECM shows relatively large underestimation of the spectral values in the frequency range of 10–0.01 Hz, while the polynomial ECM only show a small overestimation of the spectral values in the low frequency range of 0.03–0.01 Hz. From Fig. 14, it can be found that: 1) the predicted impedance spectra of both polynomial ECM and interpolation ECM match well with the experimental impedance spectra over the whole range of frequencies at 273 and 283 K; 2) both polynomial ECM and interpolation ECM show a little overestimation of the spectral values in the low-frequency range at 303 K; and 3) at the temperature of 293 K, although the polynomial ECM shows a little deviation in both medium- and low-frequency ranges, the MAPE of the proposed polynomial ECM of only 5% is acceptable for practical requirement. It is observed from Fig. 15 that: 1) the predicted impedance spectra of the polynomial ECM are almost in line with the experimental impedance spectra over the whole frequency range at different temperatures; and 2) the interpolation ECM fails to predict the true impedance spectra at temperatures of 273, 293, and 303 K. Moreover, based on a thorough analysis of all LOOCV prediction results, it is found that both polynomial ECM and interpolation ECM could provide almost accurate impedance spectra prediction at the high-frequency range, and relatively large deviations between predicted and experimental impedance spectra are mostly observed at the medium- and low-frequency range. It might imply that the charge transfer and solid-state lithium-ion diffusion processes-related impedance spectrum is more difficult to be modeled. The possible reason is that the charge resistance, Warburg resistance, and CPE element are difficult to be accurately predicted at unseen SOC values. Hence, based on the foregoing prediction performance comparison, it is reasonable to conclude that the proposed polynomial ECM provides an easy, reliable, and accurate way to depict the nonlinear relationship between SOC and circuit parameters, whereas the traditional interpolation method might fail to predict the true circuit parameters with unseen SOC at some frequency ranges.

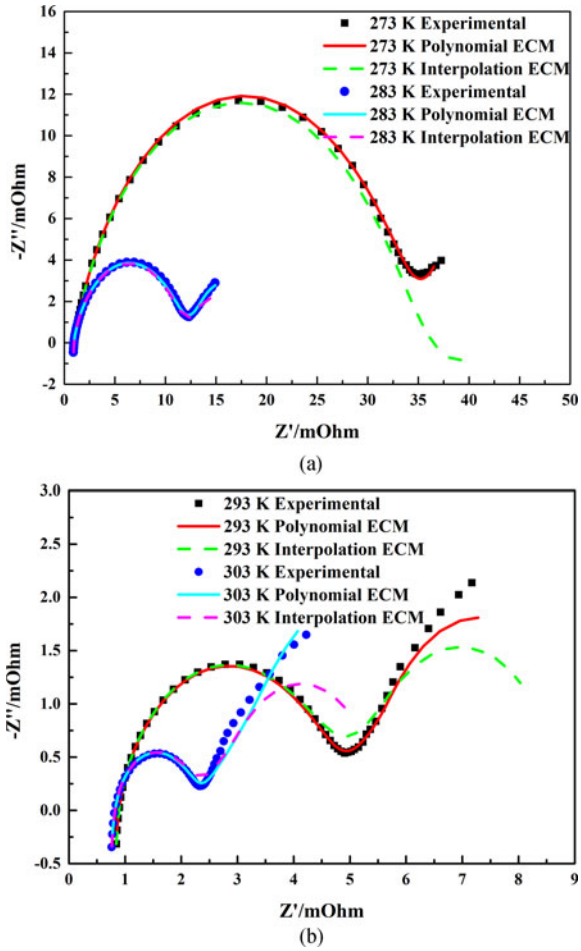


Fig. 15. Predicted impedance spectra with 90% SOC using the polynomial ECM and interpolation ECM at different temperatures.

Note that although the effectiveness of the proposed polynomial ECM approach has only been validated by a commercial pouch-type $LiFePO_4$ battery, the ECM structure shown in Fig. 2 might be different for other battery technologies. However, the proposed polynomial-based modeling approach provides a universal modeling strategy for embedding the SOC effect on the circuit parameters. In addition, the LOOCV method could provide a potential effective way for selecting suitable polynomial order.

## V. Conclusion

In this paper, a polynomial ECM conscious of SOC effect, consisting of inductance, ohmic resistance, charge resistance, Warburg element, and CPE element, is proposed to model impedance spectra. A commercial 20-A·h $LiFePO_4$ battery is used to experimentally investigate the impacts of SOC and temperature on impedance spectra and circuit parameters. The proposed ECM with SOC-dependent circuit parameters modeled by polynomial functions is used to fit EIS data at different SOC, and the effect of polynomial function order is thoroughly investigated. The fitting results of the polynomial ECM demonstrate that the analytical polynomial function can effectively capture the nonlinear relationship between SOC and circuit parameters. Moreover, the most suitable polynomial function order for modeling the SOC effect on circuit parameters is determined by the LOOCV method. The LOOCV prediction results demonstrate that the polynomial ECM is able to finely fit the experimental impedance spectra and is far superior to the common interpolation-based counterpart.

## References

[1] J. M. Tarascon and M. Armand, "Issues and challenges facing rechargeable lithium batteries," *Nature*, vol. 414, no. 6861, pp. 359–367, Nov. 2001.
[2] T. M. Bandhauer, S. Garimella, and T. F. Fuller, "A critical review of thermal issues in lithium-ion batteries," *J. Electrochem. Soc.*, vol. 158, no. 3, pp. R1–R25, Jan. 2011.
[3] V. Etacheri, R. Marom, R. Elazari, G. Salitra, and D. Aurbach, "Challenges in the development of advanced Li-ion batteries: A review," *Energy Environ. Sci.*, vol. 4, no. 9, pp. 3243–3262, Sep. 2011.
[4] B. Scrosati, J. Hassoun, and Y. K. Sun, "Lithium-ion batteries. A look into the future," *Energy Environ. Sci.*, vol. 4, no. 9, pp. 3287–3295, Sep. 2011.
[5] W. Waag, C. Fleischer, and D. U. Sauer, "Critical review of the methods for monitoring of lithium-ion batteries in electric and hybrid vehicles," *J. Power Sources*, vol. 258, pp. 321–339, Jul. 2014.
[6] Y. Xing, E. W. M. Ma, K. L. Tsui, and M. Pecht, "Battery management systems in electric and hybrid vehicles," *Energies*, vol. 4, no. 11, pp. 1840–1857, Nov. 2011.
[7] L. Lu, X. Han, J. Li, J. Hua, and M. Ouyang, "A review on the key issues for lithium-ion battery management in electric vehicles," *J. Power Sources*, vol. 226, pp. 272–288, Mar. 2013.
[8] M. Dubarry, C. Truchot, A. Devie, and B. Y. Liaw, "State-of-charge determination in lithium-ion battery packs based on two-point measurements in life," *J. Electrochem. Soc.*, vol. 162, no. 6, pp. A877–A884, Jan. 2015.
[9] S. Lee, J. Kim, J. Lee, and B. H. Cho, "State-of-charge and capacity estimation of lithium-ion battery using a new open-circuit voltage versus state-of-charge," *J. Power Sources*, vol. 185, no. 2, pp. 1367–1373, Dec. 2008.
[10] M. Charkhgard and M. Farrokhi, "State-of-charge estimation for lithium-ion batteries using neural networks and EKF," *IEEE Trans. Ind. Electron.*, vol. 57, no. 12, pp. 4178–4187, Dec. 2010.
[11] V. Klass, M. Behm, and G. Lindbergh, "Evaluating real-life performance of lithium-ion battery packs in electric vehicles," *J. Electrochem. Soc.*, vol. 159, no. 11, pp. A1856–A1860, Jan. 2012.
[12] Y. J. He, J. N. Shen, J. F. Shen, and Z. F. Ma, "State of health estimation of lithium-ion batteries: A multiscale Gaussian process regression modeling approach," *AIChE J.*, vol. 61, no. 5, pp. 1589–1600, May 2015.
[13] X. S. Hu, S. B. Li, and H. Peng, "A comparative study of equivalent circuit models for Li-ion batteries," *J. Power Sources*, vol. 198, pp. 359–367, Jan. 2012.
[14] M. Takahashi, S. I. Tobishima, K. Takei, and Y. Sakurai, "Reaction behavior of $LiFePO_4$ as a cathode material for rechargeable lithium batteries," *Solid State Ion.*, vol. 148, nos. 3/4, pp. 283–289, Jun. 2002.
[15] J. Illig, M. Ender, T. Chrobak, J. P. Schmidt, D. Klotz, and E. Ivers-Tiffée, "Separation of charge transfer and contact resistance in $LiFePO_4$-cathodes by impedance modeling," *J. Electrochem. Soc.*, vol. 159, no. 7, pp. A952–A960, Jul. 2012.
[16] J. Xu, C. C. Mi, B. Cao, and J. Cao, "A new method to estimate the state of charge of lithium-ion batteries based on the battery impedance model," *J. Power Sources*, vol. 233, pp. 277–284, Jul. 2013.
[17] F. Leng, C. M. Tan, R. Yazami, and M. D. Le, "A practical framework of electrical based online state-of-charge estimation of lithium ion batteries," *J. Power Sources*, vol. 255, pp. 423–430, Jun. 2014.
[18] A. Eddahech, O. Briat, N. Bertrand, J. Y. Delétage, and J. M. Vinassa, "Behavior and state-of-health monitoring of Li-ion batteries using impedance spectroscopy and recurrent neural networks," *Int. J. Elect. Power*, vol. 42, no. 1, pp. 487–494, Nov. 2012.
[19] M. E. Orazem and B. Tribollet, *Electrochemical Impedance Spectroscopy*. Hoboken, NJ, USA: Wiley, 2008.
[20] M. D. Levi and D. Aurbach, "Simultaneous measurements and modeling of the electrochemical impedance and the cyclic voltammetric characteristics of graphite electrodes doped with lithium," *J. Phys. Chem. B*, vol. 101, no. 23, pp. 4630–4640, Jun. 1997.
[21] M. Umeda, K. Dokko, Y. Fujita, M. Mohamedi, I. Uchida, and J. R. Selman, "Electrochemical impedance study of Li-ion insertion into mesocarbon microbead single particle electrode Part 1. Graphitized carbon," *Electrochim. Acta*, vol. 47, no. 6, pp. 885–890, Dec. 2001.

[22] P. S. Attidekou, S. Lambert, M. Armstrong, J. Widmer, K. Scott, and P. A. Christensen, "A study of 40 Ah lithium ion batteries at zero percent state of charge as a function of temperature," *J. Power Sources*, vol. 269, pp. 694–703, Dec. 2014.
[23] S. Rodrigues, N. Munichandraiah, and A. K. Shukla, "A review of state-of-charge indication of batteries by means of a.c. impedance measurements," *J. Power Sources*, vol. 87, nos. 1/2, pp. 12–20, Apr. 2000.
[24] J. Gomez, R. Nelson, E. E. Kalu, M. H. Weatherspoon, and J. P. Zheng, "Equivalent circuit model parameters of a high-power Li-ion battery: Thermal and state of charge effects," *J. Power Sources*, vol. 196, no. 10, pp. 4826–4831, May 2011.
[25] S. S. Zhang, K. Xu, and T. R. Jow, "Electrochemical impedance study on the low temperature of Li-ion batteries," *Electrochim. Acta*, vol. 49, no. 7, pp. 1057–1061, Mar. 2004.
[26] P. Suresh, A. K. Shukla, and N. Munichandraiah, "Temperature dependence studies of a.c. impedance of lithium-ion cells," *J. Appl. Electrochem.*, vol. 32, no. 3, pp. 267–273, Mar. 2002.
[27] W. G. Wang, H. S. H. Chung, and J. Zhang, "Near-real-time parameter estimation of an electrical battery model with multiple time constants and SOC-dependent capacitance," *IEEE Trans. Power Electron.*, vol. 29, no. 11, pp. 5905–5920, Nov. 2014.
[28] P. L. Moss, G. Au, E. J. Plichta, and J. P. Zheng, "An electrical circuit for modeling the dynamic response of Li-ion polymer batteries," *J. Electrochem. Soc.*, vol. 155, no. 12, pp. A986–A994, Oct. 2008.
[29] J. R. Macdonald, "Note on the parameterization of the constant-phase admittance element," *Solid State Ion.*, vol. 13, no. 2, pp. 147–149, 1984.
[30] M. Doyle, J. P. Meyers, and J. Newman, "Computer simulations of the impedance response of lithium rechargeable batteries," *J. Electrochem. Soc.*, vol. 147, no. 1, pp. 99–110, 2000.
[31] A. Lasia, *Electrochemical Impedance Spectroscopy and Its Applications*. New York, NY, USA: Springer, 2014.
[32] T. Hastie, R. Tibshirani, and J. Friedman, *The Elements of Statistical Learning*. New York, NY, USA: Springer, 2009.

**Qian-Kun Wang** received the B.Sc. degree in chemical engineering from Shanghai Jiao Tong University, Shanghai, China, in 2015, where he is currently working toward the Ph.D. degree in applied chemistry in the Department of Chemical Engineering.

His research interests include modeling and optimization of energy storage systems.

**Yi-Jun He** received the B.Sc. and Ph.D. degrees in chemical engineering from Zhejiang University, Hangzhou, China, in 2003 and 2008, respectively.

He is currently an Associate Professor with the Department of Chemical Engineering, Shanghai Jiao Tong University, Shanghai, China. He was a Postdoctoral Researcher with the Department of Chemical Engineering, Zhejiang University, between 2008 and 2010. He was also a Visiting Scholar with the Department of Chemical Engineering, Carnegie Mellon University, Pittsburgh, PA, USA, between 2013 and 2014. His research interests include modeling, optimization, and control of complex industrial systems.

**Jia-Ni Shen** received the B.Sc. and Ph.D. degrees in chemical engineering from Shanghai Jiao Tong University, Shanghai, China, in 2006 and 2017, respectively, and the M.Sc. degree in chemical engineering from the Dalian Institute of Chemical Physics, Chinese Academy of Sciences, Dalian, China, in 2009.

She is currently an Assistant Professor with the Department of Chemical Engineering, Shanghai Jiao Tong University. Her research interests include modeling, optimization, and monitoring of energy storage systems.

**Xiao-Song Hu** (SM'16) received the Ph.D. degree in automotive engineering from the Beijing Institute of Technology, Beijing, China, in 2012. He did scientific research and completed the Ph.D. dissertation in the Automotive Research Center, University of Michigan, Ann Arbor, MI, USA, between 2010 and 2012.

He is currently a Professor with the State Key Laboratory of Mechanical Transmissions and with the Department of Automotive Engineering, Chongqing University, Chongqing, China. He was a Postdoctoral Researcher with the Department of Civil and Environmental Engineering, University of California, Berkeley, CA, USA, between 2014 and 2015, as well as with the Swedish Hybrid Vehicle Center and the Department of Signals and Systems, Chalmers University of Technology, Gothenburg, Sweden, between 2012 and 2014. He was also a Visiting Postdoctoral Researcher with the Institute for Dynamic Systems and Control, Swiss Federal Institute of Technology, Zurich, Switzerland, in 2014. His research interests include modeling and control of alternative-energy powertrains and energy storage systems.

Dr. Hu has been a recipient of several prestigious awards/honors, including the Emerging Sustainability Leaders Award in 2016, the EU Marie Currie Fellowship in 2015, the American Society of Mechanical Engineers Dynamic Systems and Control Division Energy Systems Best Paper Award in 2015, and the Beijing Best Ph.D. Dissertation Award in 2013.

**Zi-Feng Ma** received the B.Sc. and M.Sc. degrees in chemical engineering from Zhejiang University, Hangzhou, China, in 1985 and 1988, respectively, and the Ph.D. degree in chemical engineering from the South China University of Technology, Guangdong, China, in 1995.

He is currently a Distinguished Professor with the Department of Chemical Engineering, Shanghai Jiao Tong University, Shanghai, China, and the founding Director of Shanghai Electrochemical Energy Devices Research Centre, Shanghai. He was the Chair of the Department of Chemical Engineering, Shanghai Jiao Tong University, from 1999 to 2011. He was appointed to be the Chief Scientist of the National Basic Research Program of China for electrochemical energy system in 2007 and 2013. His research interests include development of advanced energy materials and electrochemical energy systems for electric vehicle and energy storage applications.

Dr. Ma was a 2016 recipient of the China Industry-University-Research Collaborative Award.